Analyzed electrical performance and induced interface passivation of fabricated Al/NTCDA/p-Si MIS–Schottky heterojunction

Ahmed M. Nawar[1,2] · Mohamed Abd-Elsalam[1] · Ahmed M. El-Mahalawy[1] · M. M. El-Nahass[3]

Abstract

In this research, the significant role of 1,4,5,8-naphthalenetetracarboxylic-dianhydride, NTCDA, thin film on the Al/p-Si barrier under different temperatures is investigated. The structural and topographical properties of the thermally evaporated NTCDA thin film are investigated using a transmission electron microscope, TEM, and atomic force microscope, AFM, respectively, and elucidated that the fabricated films have a smooth nanocrystalline nature with an average crystallite size about 89 nm and average roughness about 3.15 nm. Furthermore, the current–voltage (I–V) characteristics of Al/NTCDA/p-Si/Al device are studied under dark conditions at different temperatures (313–383 K). The Schottky diode electronic parameters such as ideality factor, n, barrier height, Φ_B, and reverse saturation current, I_s, are calculated at each temperature. A clear increment of Φ_B from 0.74 to 0.88 eV accompanied by a clear decrement of n values from 5.83 to 4.99 under increasing temperature (313–383) K is noticed. Due to the inhomogeneity of barrier height, the Gaussian distribution of Schottky barrier height is employed to estimate the mean value of barrier height and standard deviation and found to be 1.5 eV and 20 mV, respectively. The modified Richardson plot is used to estimate the modified Richardson constant and found to be 35.2 A cm^{-2} K^{-2} which is close to the known value of p-Si. Moreover, the conduction mechanism in forward and reverse biasing is explained in details. The modified Norde's function is employed for estimating the series resistance, R_s, and barrier height of the fabricated device at each temperature, where the values of R_s showed a decrement behavior from 3.564 to 1.165 kΩ upon increasing the temperature. The process of inserting NTCDA between electrode and p-Si influenced the distribution of interface states for MIS Schottky diode at different temperatures and is explained as a passivation process of the device's interface states.

Keywords NTCDA · Schottky barrier · Norde's model · Interface state density

1 Introduction

Through the last decades, there were intensive efforts for replacing the inorganic semiconductors by organics in most of the electronic applications. Organic semiconductors

overcome many of inorganic disadvantages such as high cost on a large scale in either preparation or device fabrication and the low compatibility with flexible substrates [1]. The high optical absorption, high flexibility, and the ability to tune the electronic and optoelectronic properties of the material by controlling the molecular structure make these materials promising for a wide scale of potential applications [1–3]. Although the (opto-)electronic devices based on organic semiconductors have emerged the electronic devices markets until now, inorganic semiconductors are favorable for most of the sophisticated electronic applications [4, 5]. In this framework, one can notice a great acceleration in the field of scientific researches concerning the material science and characterization of organic semiconductors aiming to modify their properties for eventually recording a high-performance efficiency of the electronic device. Among the different categories of organic semiconductors,

✉ Ahmed M. Nawar
  nawarphysics@yahoo.com; anawar@bu.edu.sa;
  ahmed_nawar@science.suez.edu.eg

1   Thin Films Laboratory, Physics Department, Faculty of Science, Suez Canal University, Ismailia 41522, Egypt

2   Physics Department, Faculty of Science and Arts (AlMikhwah), AlBaha University, Al Baha, Kingdom of Saudi Arabia

3   Thin Films Laboratory, Physics Department, Faculty of Education, Ain Shams University, Roxy 11757, Cairo, Egypt

two-dimensional organic oligomers attract great interest in many applications due to their planar structure and conjugation that cause higher electronic delocalization [6, 7].

1,4,5,8-Naphthalenetetracarboxylic-dianhydride with a planar π-stacking structure has emerged as a promising material for the organic electronics community. Over the past years, NTCDA attracted the attention of many researchers with the aim to study the epitaxial growth of several monolayers of this molecule, organic–inorganic hybrid complexation, and degradation mechanisms [8–19]. Among several n-type materials, NTCDA is considered one of the most promising organic semiconductors due to its high mobility, high air stability, and strong photocurrent gain in optical photodetectors [20–24]. Moreover, according to the innate nature of high absorption of NTCDA, this is a significant property that qualifies it to be utilized as an active layer in photodiode applications [25–27]. In this sense, NTCDA was exploited in a wide range of electronic and optoelectronic applications including organic solar cells [28, 29]. The NTCDA thin film of thickness (30–50) nm have played rules as an optical spacer and electron transport layer (ETL) in organic solar cell of the following architecture [ITO/ novaled p-dopant 2/N,N,N,N-tetrakis(4-methoxyphenyl)-benzidine/zinc-phthalocyanine-doped fullerene (1:1)/fullerene/NTCDA:acridine orange base (20:1)/AL] showed a clear enhancement in the cell efficiency reaching the maximum value 2.83% at thickness 30 nm [28]. Furthermore, NTCDA was exploited with 3,4,9,10 perylenetetracarboxylic bisbenzimidazole (PTCBI) due to the equality of LUMO position of both (~ 4 eV) for modifying the organic solar cell based on 2,4-bis[4-(N-phenyl-1-naphthylamino)-2,6-dihydroxyphenyl] squaraine/fluorine and showed efficiency enhancement by > 25% relative to the conventional architectures that use bathocuproine [29]. NTCDA is considered as one of the common n-type materials that are used in n-channel organic field-effect transistors (OFETs) [20, 30-32] and recorded a charge mobility ~ 0.016 cm^2 V^{-1} s^{-1}, voltage threshold ~ 32 V, cut-off current ~ 1.76 nA, and saturation on/off ratio ~ 2.25×10^2 at (drain–source voltage = 60 V) [30]. Organic diodes based on NTCDA/polypyrrole and NTCDA/poly(3,4-ethylenedioxythiophene) doped with poly(styrenesulfonate) showed a rectification behavior of rectification ratio ~ 4.1×10^3 and break down at 9 V with turn-on voltage ~ 1.2 and 1.7 V, respectively [33]. After the first deep investigation of photocurrent multiplication in NTCDA [34], NTCDA becomes a favorable applicable material for photodetection devices. Therefore, much previous work concerned the exploitation of NTCDA with p-type organic semiconductor for optoelectronic applications, where NTCDA/PTCDA multiple quantum well-organic photodetector [35] and NTCDA/phthalocyanine heterojunction light sensor [36] achieved a good performance. Interestingly, NTCDA showed a decisive role in enhancing the performance of organic light-emitting diodes (OLEDs) based on ITO/NPB/Alq$_3$ + C54T/Alq$_3$/LiF/Al, when inserted between ITO and NPB for enhancing the process of hole injection due to the strong interaction between NTCDA and ITO that lowers the barrier for holes that transfer from ITO to hole transporting layer (NPB) [37]. The process of insertion NTCDA thin layer (3 nm) between ITO and NPB achieved a decrement of operating voltage of OLED from 12.2 to 9.2 V ($J \sim 100$ mA cm^{-2}) which gives rise to 10^4 cd cm^{-2} luminance.

Despite the growing interest in the physical properties of this compound and how to exploit it in a lot of architectures as an effective n-type material to achieve high efficiency, there is no previous work concerned exploring the nature of inter layering NTCDA in metal/semiconductor, MS, and Schottky diode. Hence, this research focuses on the role of NTCDA thin film on the performance of the Al/p-Si Schottky diode. According to the high thermal stability of NTCDA, as obtained in our previous work [26], the performance of the fabricated Schottky diode is investigated in the temperature range (303–383) K.

2 Experimental work

2.1 Schottky diode fabrication procedures

The architecture of the fabricated Schottky diode is shown in Fig. 1a. 1,4,5,8-Naphthalenetetracarboxylic-dianhydride, NTCDA, (C$_{14}$H$_4$O$_6$) powder purchased from Alfa Aeser Company of chemical structure that is shown in Fig. 1b is our raw material. A thin film of NTCDA of thickness 150 nm was deposited on chemically pre-etched p-type silicon substrates of orientation [111] and resistivity (8–13 Ω cm) using thermal evaporation technique (coating unit Edwards 306A-England) at room temperature under pressure 3×10^{-5} mbar. The deposition rate and film thickness were controlled using the quartz crystal monitor thickness model Edward FTM6 to be 0.2 nm s^{-1} and 150 nm, respectively. Then, a 100 nm aluminum top electrode was deposited on NTCDA thin film using a shadow mask in the form of a mesh. Finally, a thick-aluminum bottom electrode of thickness 300 nm was deposited on the backside of Si.

2.2 Characterization techniques

Atomic Force Microscope, AFM, operated in contact mode using a nonconductive silicon nitride probe, manufactured by Bruker (Model: MLCT-MT-A) was employed to investigate the surface topography of NTCDA as-deposited thin film. The scan area under study was 5×5 μm^2 with 1 Hz scan rate. The microstructural properties of the prepared thin film were investigated using a high-resolution

Fig.1 **a** Architecture of the fabricated *Schottky* diode, **b** molecular structure of NTCDA, and **c**, **d** 3D AFM image of as-deposited NTCDA thin film
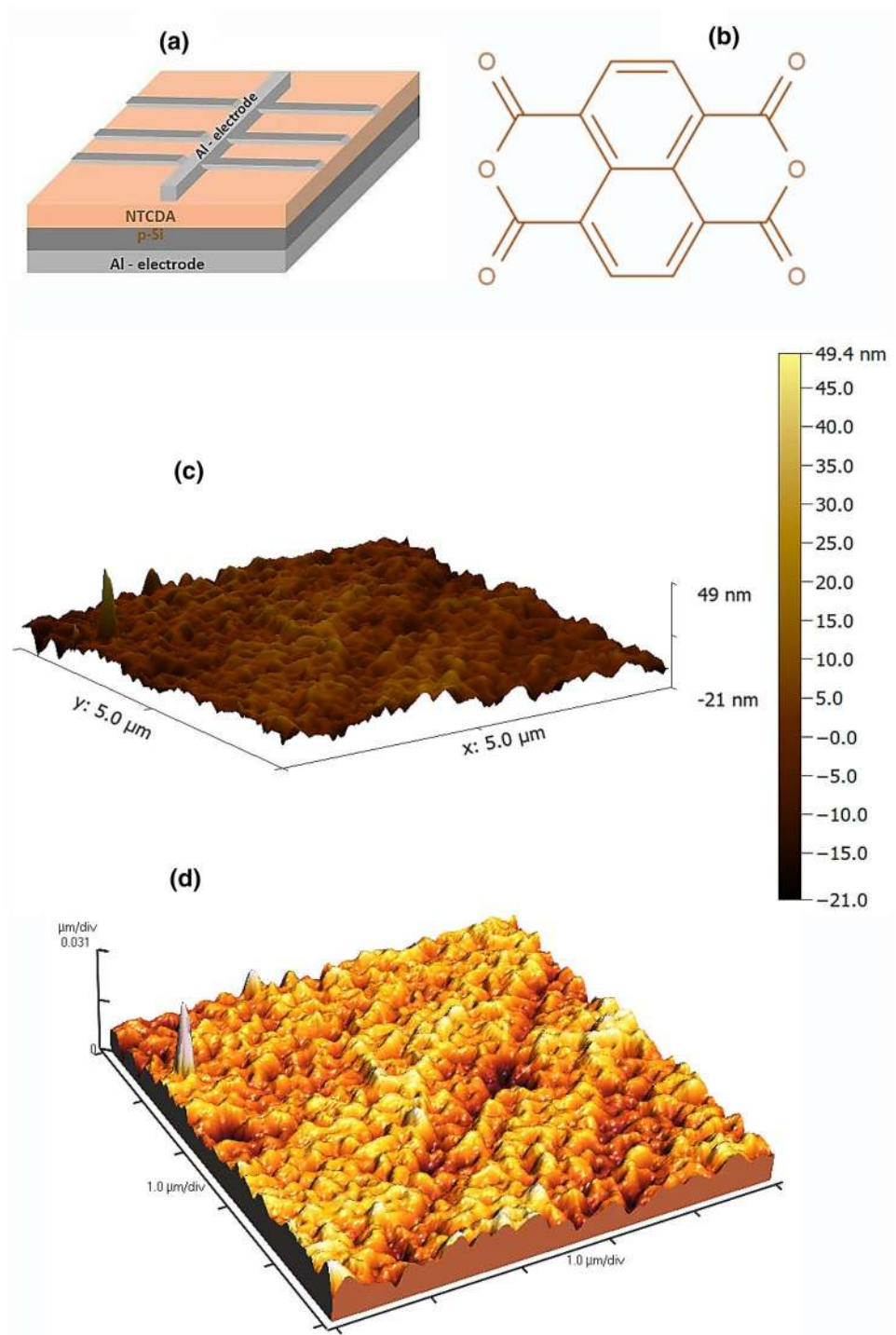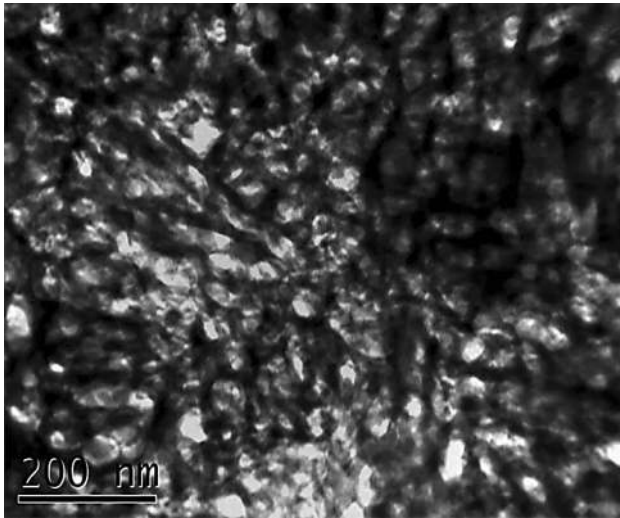
transmission electron microscope, TEM; model JEOL-JEM-HR-2100 with accelerating voltage 200 kV. The obtained TEM images were in DM3 format and were analyzed using ImageJ software. The electrical properties of the fabricated Al/NTCDA/p-Si/Al diode were investigated by measuring the *I–V* characteristic curve under the dark conditions from -2.5 to $+2.5$ V using Keithley electrometer model 6517B at different temperatures ranges from 313 to 383 K.

3 Results and discussion

3.1 Topographical and microstructural properties of NTCDA thin films

The surface roughness of organic interfacial thin film is a primary factor that has a significant impact on the performance of any electronic device [38–40], where surface

nanoroughness induces surface defects that play an important role in charge dynamics and recombination rate at surface [41]. Hence, the surface topography of NTCDA thin film was inspected using the atomic force microscope. The AFM images of NTCDA thin film that is shown in Fig. 1c, d reveal the granular nature of the NTCDA surface with a root-mean-square roughness and average roughness about 4.05 nm and 3.15 nm, respectively. The small values of roughness parameters clarify the validity and suitability of forming a smooth interfacial contact between NTCDA and the metal

electrode which enhances the performance of any electronic device [42, 43].

Furthermore, the microstructural properties of the organic interlayer film between the semiconductor and metal electrode have essential importance for achieving output performance outstanding [44]. In this essence, the microstructural properties of NTCDA thin film are studied using TEM. Figure 2 reveals the TEM image of NTCDA thin film and shows a good quality crystallized structure with small molecular crystals arranged with a definite grain boundary. There is a distribution of pores with different dimensions. The average crystallite size as estimated from TEM is about 89 nm.

3.2 Current–voltage characteristics

Figure 3 shows the temperature-dependent *I–V* characteristics of the fabricated Schottky diode. The observed electrical response shows rectification behavior with a room temperature–rectification ratio of 4.6 at ± 2 V. The forward current increases linearly at low forward biasing voltages, and then under the influence of the high series resistance, the device behavior deviates from linearity to an exponential growth behavior. It is clear that the temperature variation has a significant impact on the electrical properties of the fabricated device. The increment of the produced current with increasing the temperature at a certain constant voltage indicates the negative temperature coefficient of resistivity [45]. The cut-in voltage of the fabricated device ranged from 1.3 to 1.19 V as the temperature increases from 303 to 383 K.

Fig.2 The TEM micrograph of As-deposited NTCDA thin film

Fig.3 *I–V* characteristic curve of Al/NTCDA/p-Si/Al Schottky diode, while the inset represents the semi-logarithmic *I–V* relation at different temperatures
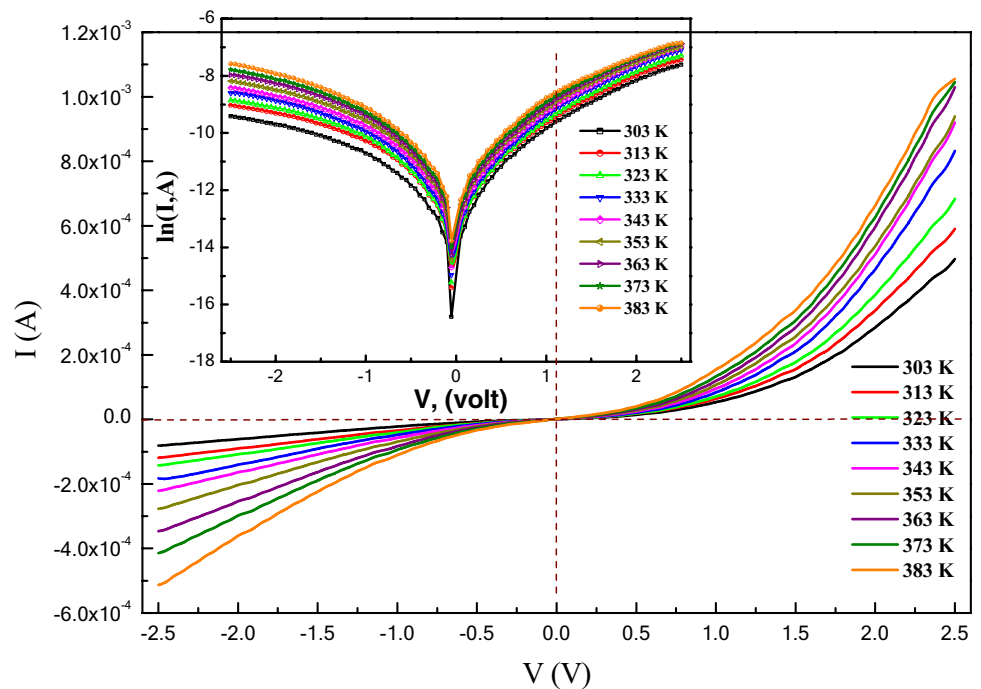
The sensitivity of the fabricated Schottky diode toward the temperature variation is discussed in terms of temperature coefficient (TC) of either voltage or current [46]. The TC value can be estimated from $d[\ln S(T)]/dT$, where $S(T)$ can be represented as forward current, I_F, or forward voltage, V_F [46]. Figure 4a, b represents the temperature dependence of forward current and voltage, respectively. The estimated values of the temperature coefficient of current ranges from 1.24 to 0.92% K^{-1} at voltage range from 0.5 to 2.5 V as revealed in Fig. 4a, while the temperature

coefficient of voltage ranges from -0.59 to -0.41% K^{-1} at current range from 0.1 to 0.5 mA as revealed in Fig. 4b.

Figure 5 depicts the semi-logarithmic relation between voltage and current in forward biasing state at different temperatures. Three distinct regions are clearly observed: region **I** at $V < 0.35$ V, region **II** at $0.35 < V$ $V < 1.2$ V, and region **III** at $V > 1.2$ V.

The thermionic emission model can be utilized to fit the linear current–voltage behavior in the low biasing region (region **I**). According to thermionic emission theory, the temperature dependence of I–V relation of organic/

Fig.4 The temperature dependence of **a** $\ln I_F$ and **b** $\ln V_F$ for estimating *TC*
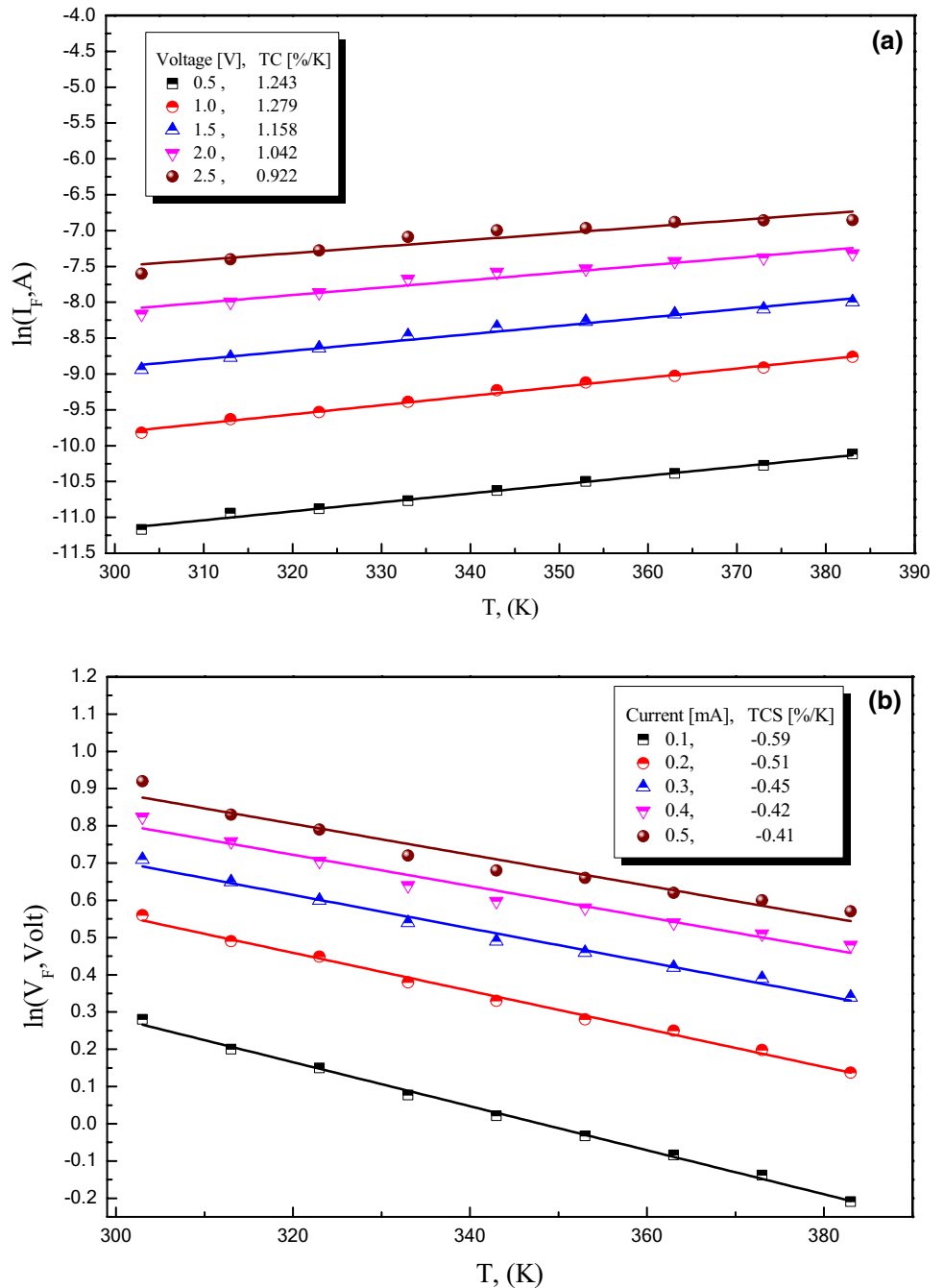
Fig.5 Semi-logarithmic plot of *I–V* characteristics of Al/NTCDA/p-Si/Al Schottky at different temperatures
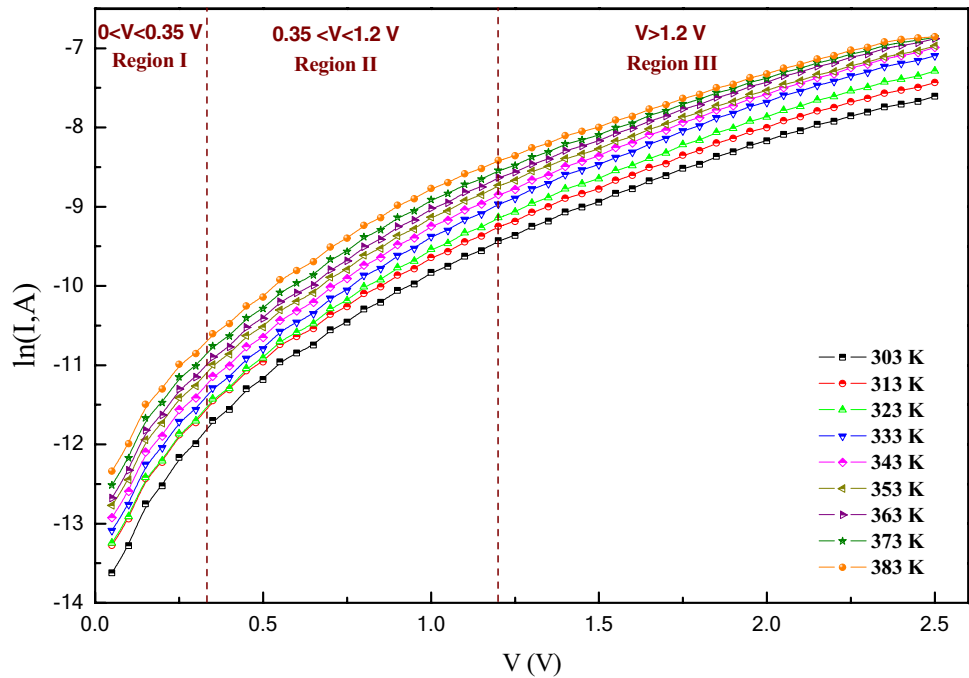
inorganic heterojunction is represented by the following relation [47, 48]:

$$I = I_s \exp\left(\frac{q(V - IR_s)}{nk_BT}\right)\left[1 - \exp\left(\frac{-q(V - IR_s)}{k_BT}\right)\right],$$

(1)

where I_s is the reverse saturation current, n is the ideality factor, q is electron charge, k_B is Boltzmann constant, T is the temperature, and R_s is the series resistance. The reverse saturation current can be represented as [47, 48]:

$$I_s = AA^*T^2 \exp\left(\frac{-q\Phi_{Bo}}{k_BT}\right),$$

(2)

where A is the device area, A^* is the effective Richardson constant, and Φ_{Bo} is the barrier height at zero bias voltage which can be estimated using the following relation:

$$\Phi_{B0} = \frac{k_BT}{q}\ln\left(\frac{AA^*T^2}{I_0}\right).$$

(3)

The ideality factor, n, was estimated from the slope of the linear region of the *I–V* curve in forward biasing using the following relation:

$$n = \frac{q}{k_BT}\left[\frac{dV}{d(\ln I)} - IR_s\right].$$

(4)

The voltage across the series resistance in the low-voltage region $V_F < 0.35$ V is negligible; hence, Eq. (4) is simplified to be:

$$n = \frac{q}{k_BT}\left[\frac{dV}{d(\ln I)}\right].$$

(5)

Figure 6a shows the estimated values of the ideality factor and barrier height as a function of temperature. The high value of the ideality factor which is greater than unity confirms the non-ideal behavior of the fabricated device. This can be ascribed to several factors such as tunneling process [48], image-force effect [49–51], series resistance [52], inhomogeneity of barrier height, the high probability of electron–hole recombination within the depletion region [53, 54], and the existence of interface states due to the native layer results from SiO_2 [53, 54]. These high values of ideality factor were previously recorded in many applicable devices such as V_2O_5/n-Si Schottky diode ($n = 6.95$ [55]), multiple quantum well LED GaInN/GaN ($n = 5.5$ [56]), Au/PEDOT:PSS/n-Si ($n \sim 4.6$ [57]), STO/p-Si ($n = 10$ [58]), and Cu(acac)$_2$/n-Si ($n = 5.6$ [54]).

It was observed that the value of n decreases, while the value of Φ_B increases as the temperature increases which confirms the heterogeneity of barrier height. The barrier height fluctuations is a recurrent behavior which exists in all organic/inorganic heterojunction diodes [54, 59]. The decrement of the ideality factor as a result of temperature increase ensures that charge transport across the metal/semiconductor interface is temperature-dependent. Hence, the charge carrier transportation takes place at low temperatures through surmounting only the lower energy barriers by electrons leading to a high ideality factor, while

Fig.6 a The temperature dependence of ideality factor and barrier height and **b** the conventional Richardson plot of the fabricated Schottky diode
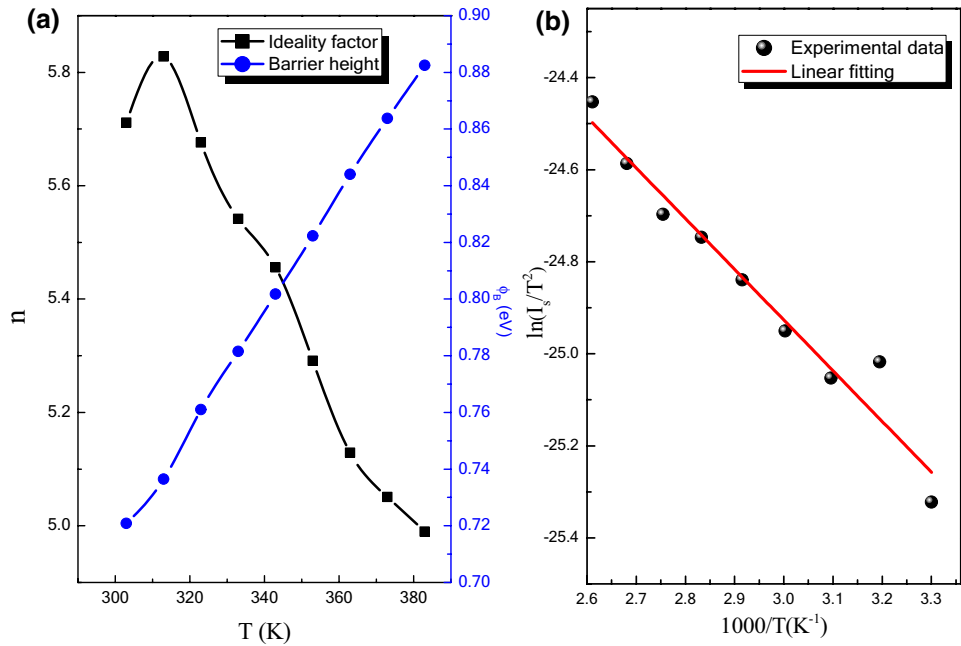
at high temperatures; electrons gained sufficient energy enough to overcome the high-energy barriers [49, 60, 61]. The insertion of the NTCDA interlayer showed a strong modification of Al/p-Si contact, where the estimated room-temperature barrier height is about 0.72 eV, which is greater than that of Al/p-Si by 0.14 eV [60].

The relation between $1000/T$ and $\ln(I_S/T^2)$ that represents the conventional Richardson plot is represented in Fig. 6b and shows a linear relation that confirms the validity of the Thermionic emission model to interpret the charge carriers conduction process of the low-voltage region.

Since the value of Schottky barrier height (SBH) is a clear manifestation of the uniformity of barrier, the temperature dependence of n and Φ_B values is investigated. The clear increment of barrier height that is shown in Fig. 6a with temperature may be attributed to the variation of the semiconductor energy gap [62]. However, according to the negative temperature coefficient of the silicon energy gap, the increase of temperature will result in a narrower energy gap and hence lower barrier height which is contrary to the current situation [49, 62]. Therefore, the Φ_B–T interrelation is not ascribed to the variation of the energy gap. The non-homogeneity of SBH was interpreted based on the assumption of a Gaussian distribution of SBH, $P(\Phi_B)$, introduced by Werner and Güttler according to the following equations [49, 62]:

$$\Phi_{B0} = \overline{\Phi}_{B0}(T=0) - \frac{q\sigma_{S0}^2}{2k_BT}, \tag{6}$$

$$n^{-1} - 1 = -\rho_2 + \frac{q\rho_3}{2k_BT}, \tag{7}$$

where $\overline{\Phi}_{B0}$ and σ_{s0} are zero-biased mean barrier height and its standard deviation, respectively, while ρ_2 and ρ_3 are constants that represent the potential deformation of distribution of SBH. Employing Eqs. (6) and (7), and based on the linear fitting of the relation between both Φ_{B0}, $n^{-1}-1$ and $q/2k_BT$ that revealed in Fig. 7a, the values of $\overline{\Phi}_{B0}, \sigma_{s0}, \rho_2$, and ρ_3 are determined and found to be 1.5 eV, 20 mV, − 0.688, and − 7.44 mV, respectively. For more confirmation, combining Eqs. (3) and (6), the conventional Richardson plot would be modified and represented as follows:

$$\ln\left(\frac{I_s}{T^2}\right) - \left(\frac{q^2\sigma_{s0}^2}{2k_B^2T^2}\right) = \ln(AA^{**}) - \frac{q\overline{\Phi}_{B0}}{k_BT}, \tag{8}$$

where A^{**} is the modified Richardson constant. From the linear fitting to Eq. (8) as shown in Fig. 7b, the mean barrier height and modified A^{**} values are estimated and found to be 1.51 eV and 35.2 A cm^{-2} K^{-2}. The estimated value of the mean value of barrier height (1.51 eV) is very close that estimated from Eq. (6) (1.5 eV), while the estimated modified Richardson constant (35.2 A cm^{-2} K^{-2}) is in a good agreement to the known value of Richardson constant of p-Si (32 A cm^{-2} K^{-2}). These coincidences confirm the validity of the thermionic emission theory and Gaussian distribution of SBHs to explain the behavior of the microelectronic parameters of Al/NTCDA/p-Si/Al Schottky diode.

The estimated high values of the ideality factor indicate that thermionic emission is no longer suitable for interpreting the transport mechanism in other voltage regions. Hence, the double logarithmic relation of forward current

Fig.7 The relation between **a**
n^{-1}–1 and Φ_{B0} versus $q/2k_BT$
and **b** $\ln(I_s/T^2) - (q^2\sigma_{s0}^2/2k_B^2T^2)$
versus q/k_BT for the fabricated
Schottky diode
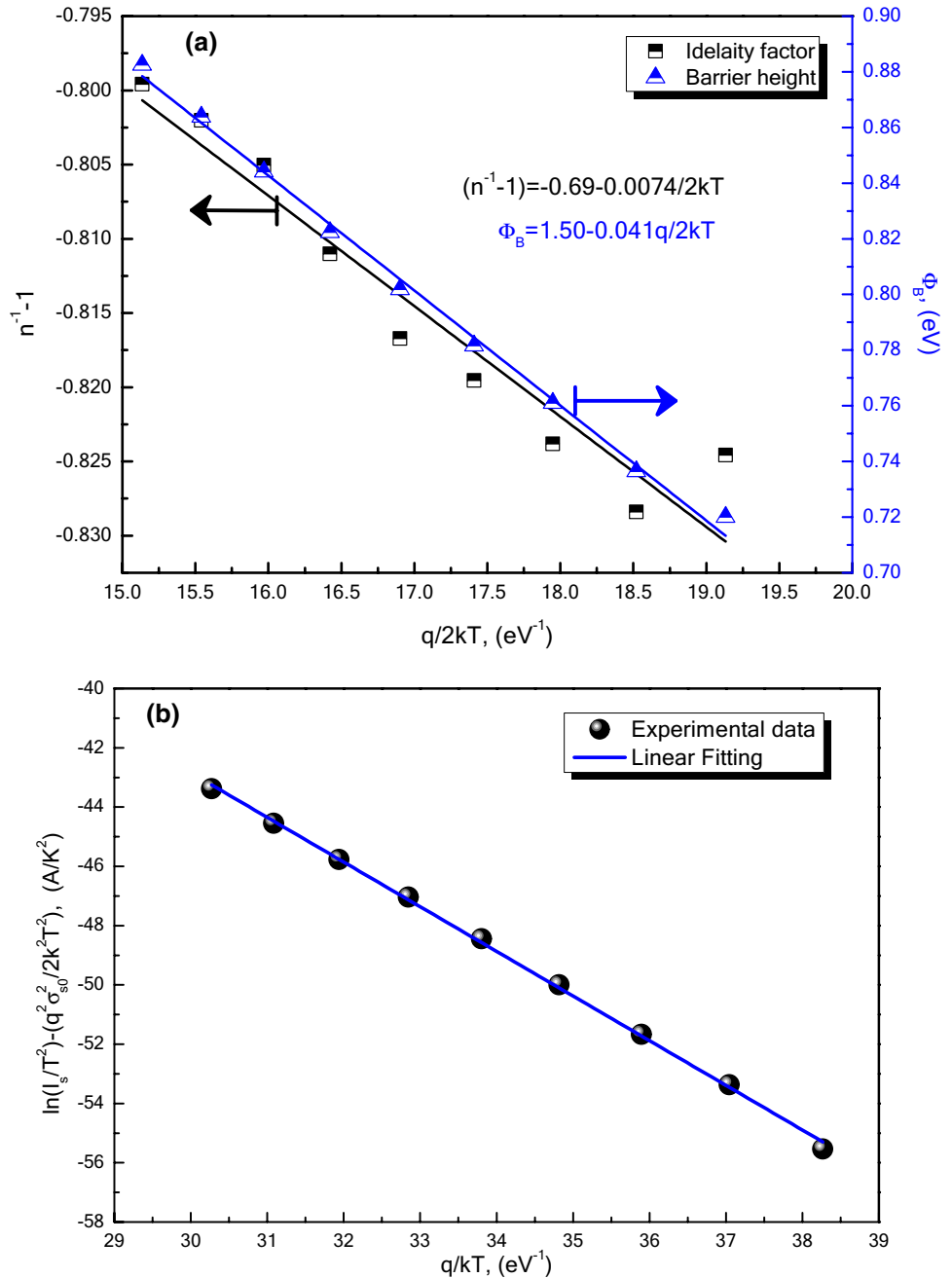
and voltage in region **II** was plotted, as shown in Fig. 8a. A set of straight lines was obtained with a slope ~2, indicating that the dominant conduction mechanism is space charge limited current (SCLC) controlled by a single trap state [53, 63]. The process of space charges injection from p-Si to NTCDA thin film takes place at the high forward biasing region, where the thin NTCDA film ultimately limits the dynamics of the charge due to low mobility. The space charge limited current can be expressed using the Mott–Gurney equation [64]:

$$I_{SC} = \frac{9}{8}\varepsilon\mu A \frac{V^2}{d^3}\frac{N_v}{N_t}\exp\left(\frac{-E_t}{k_BT}\right), \tag{9}$$

where ε is the permittivity of NTCDA film, d is the film thickness, μ is the charge carrier mobility within NTCDA film, N_v is the effective density of states located at the edge of valance band, and N_t is the total trap density at energy level E_t which locates above the valance band edge. The value of E_t is determined from the slope of $1/T$ versus $\ln I$ at different forward voltages that are depicted in Fig. 8b. The calculated average value of E_t was about 0.13 ± 0.006 eV.

Fig.8 a The variation of $\ln(I_\mathrm{F})$ versus $\ln(V)$ at different temperatures and **b** the temperature dependence of $\ln(I_\mathrm{F})$ at different voltages for Al/NTCDA/p-Si/Al diode in region **II**
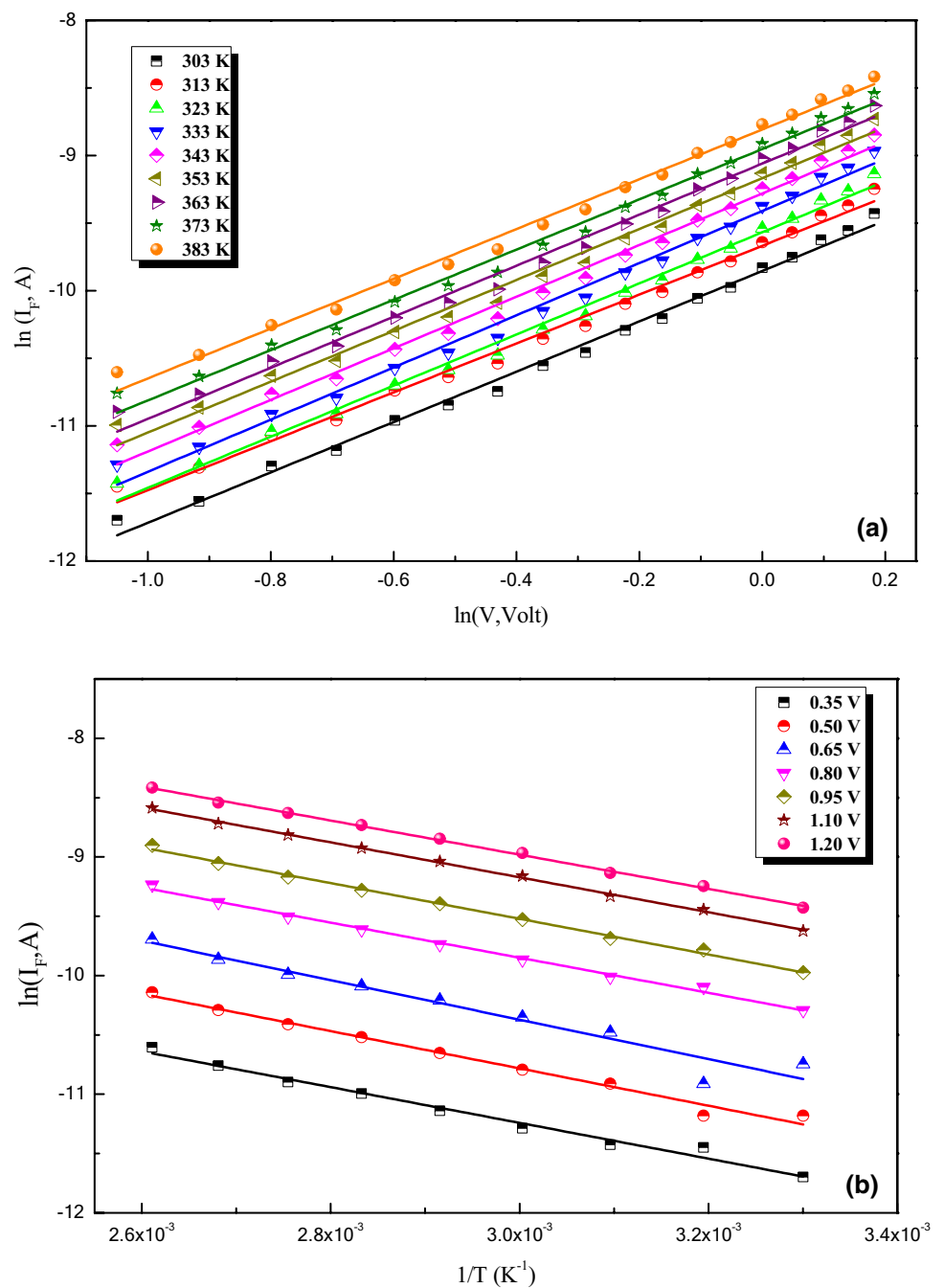
The estimated value of E_t is smaller than that was estimated for Ph-HPQ/p-Si (0.256 eV [53]), Ch-HPQ/p-Si (0.41 eV [53]), and pyronine G(Y)/p-GaAs (0.25 eV [65]), while it is close to the values of FeTPPCl/p-Si (0.1 eV [66]) and InPcCl-D/p-Si (0.11 eV [67]).

Furthermore, at higher voltage (region **III**), the slope, m, of the linear relation between $\ln(I_\mathrm{F})$ and $\ln(V)$ of the fabricated Schottky diode shown in Fig. 9a is more than 2, which suggests the space charge limited current (SCLC) dominant by an exponential trap distribution to interpret the conduction mechanism in this region [68]. In this essence, the current can be represented as follows [68–71]:

$$I = Aq\mu N_v \left(\frac{\varepsilon \varepsilon_\mathrm{o}}{e P_\mathrm{o} k_\mathrm{B} T_t} \right)^l \left(\frac{V^{l+1}}{d^{2l+1}} \right), \tag{10}$$

where P_o represents the trap density per unit energy range at the valence band edge, ε is the dielectric constant of the material ($\varepsilon = 2.89$ [72]), l is a parameter related to the slope, m, by $l = m - 1$ and represents the ratio between (T_t/T), and

Fig.9 **a** The variation of $\ln(I_F)$ versus $\ln(V)$ at different temperatures and **b** the temperature dependence of $\ln(I_F)$ at different voltages for Al/NTCDA/p-Si/Al diode in region **III**
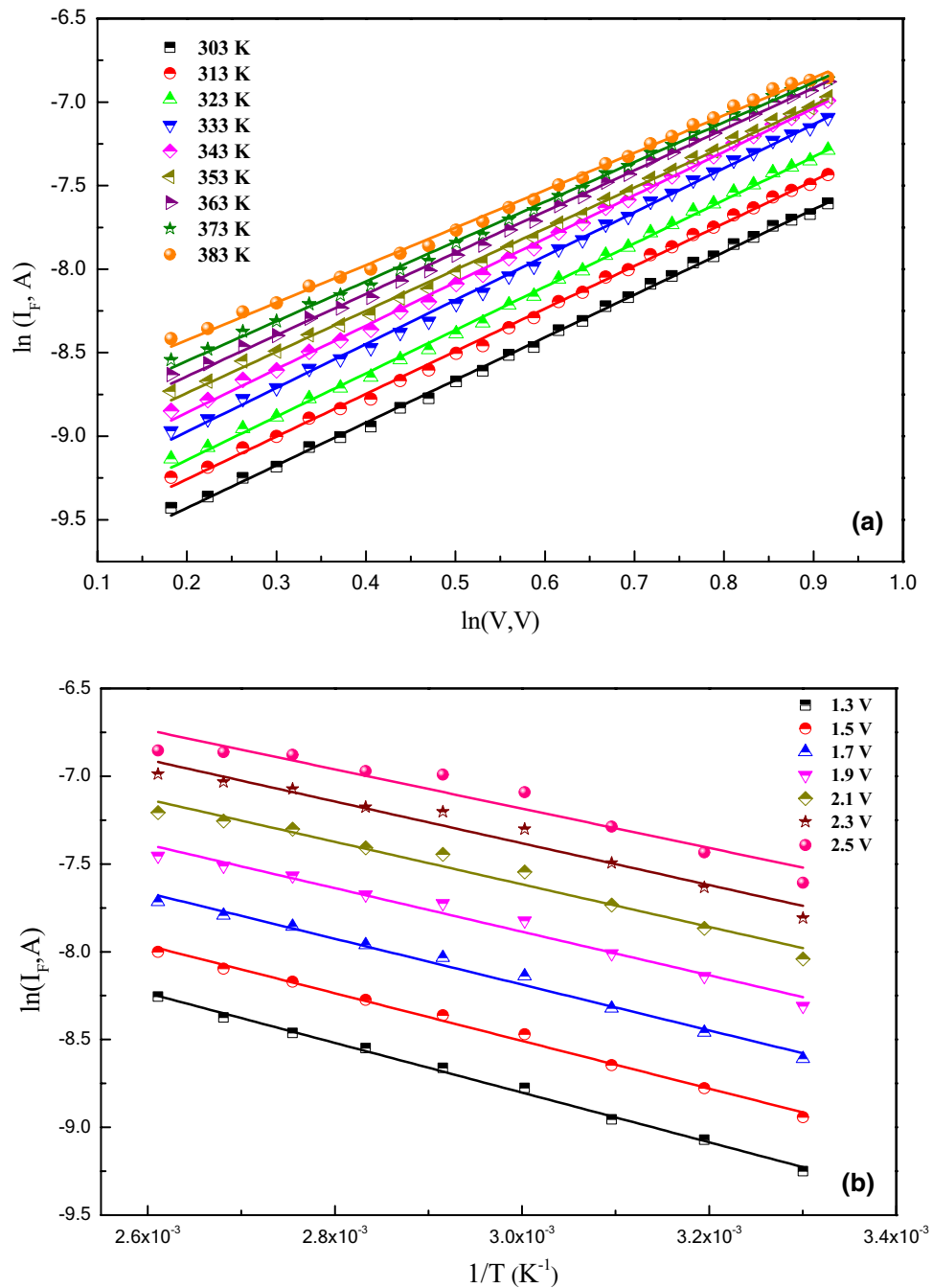
T_t is a temperature parameter describes the exponential trapping distribution $P(E)$. The values of l and T_t were calculated at different temperatures and listed in Table 1.

The exponential trap distribution function can be represented as follows [68, 71]:

$$P(E) = P_o \exp\left(\frac{-E}{k_B T_t}\right), \tag{11}$$

where $P(E)$ is trap density per unit energy at energy E over the edge of valance band. Hence, the total trap density, N_t,

can be estimated by integrating Eq. (11) and is given by [68, 71]:

$$N_{t(e)} = P_o k_B T_t. \tag{12}$$

The values of both P_o and N_t were determined at room temperature and different voltages using the obtained slope values of the linear relation between $1/T$ and $\ln(I_F)$ that is shown in Fig. 9b:

Table 1 The estimated diode parameters at different temperatures

T (K)	n	Φ_B (eV)	Φ_B (eV)	R_s (kΩ)	m	l	Tt
		TE model	Norde's model		Region III		
303	5.71	0.72	0.71	3.713	2.55	1.55	469.65
313	5.83	0.74	0.73	3.564	2.55	1.55	485.15
323	5.68	0.76	0.75	3.315	2.59	1.59	513.57
333	5.54	0.78	0.77	3.283	2.63	1.63	542.79
343	5.46	0.80	0.79	2.879	2.60	1.60	548.80
353	5.29	0.82	0.81	2.749	2.46	1.46	515.38
363	5.13	0.84	0.83	2.603	2.47	1.47	533.61
373	5.05	0.86	0.83	2.225	2.38	1.38	514.74
383	4.99	0.88	0.86	1.165	2.24	1.24	474.42

$$\text{Slope} = \frac{\Delta \ln I}{\Delta(1/T)} = T_t \ln\left(\frac{\varepsilon V}{q d^2 N_{t(e)}}\right). \tag{13}$$

The estimated values of P_o were about 2.89×10^{44} J^{-1} m^{-3}, 2.99×10^{44} J^{-1} m^{-3}, and 2.97×10^{44} J^{-1} m^{-3}, while N_t values were about 1.88×10^{24} m^{-3}, 1.94×10^{24} m^{-3}, and 1.92×10^{24} m^{-3} at 1.3, 1.5, and 2.5 V, respectively. These values are smaller than those that were estimated for TiOPc/p-Si [66]. The globally distributed trap density lowers the anode injection barrier, where the trapped states which are filled with injected carriers from anode enhance the screening effect that gives rise to band bending and reducing the potential difference between anode and cathode neglecting the hypotheses of the linear I–V relation [73].

The reverse current shows a strong temperature dependence, as shown in Fig. 3, which emphasizes that the leakage current is controlled by the generation–recombination of thermally activated charge carriers with Si substrate [68, 74, 75]. The dependence of reverse current, I_R, on thermal activation energy, ΔE, of the charge carriers is given by [68, 74]:

$$I_R = I_{0R} \exp\left(\frac{-\Delta E}{k_B T}\right). \tag{14}$$

The estimated values of activation energy from the linear fitting of $1/T$ and $\ln(I_R)$ relation that is depicted in Fig. 10 were about 0.199 eV which indicates that the conduction transport mechanism is tunneling of charge carriers [76].

The conduction mechanism within the Al/NTCDA/p-Si/Al Schottky diode during reverse biasing can be ascribed in terms of either Schottky emission or Poole–Frenkel emission model [45, 77]. Figure 11 depicts the relation between $V_R^{1/2}$ and $\ln(I_R)$ of the fabricated device at different temperatures and shows two linear regions of different slopes. According to Schottky conduction mechanism, the reverse current can be represented as follows [45, 77]:

Fig.10 The plot $\ln(I_R)$ versus $1/T$ of Al/NTCDA/p-Si/Al Schottky diode at different reverse bias voltages
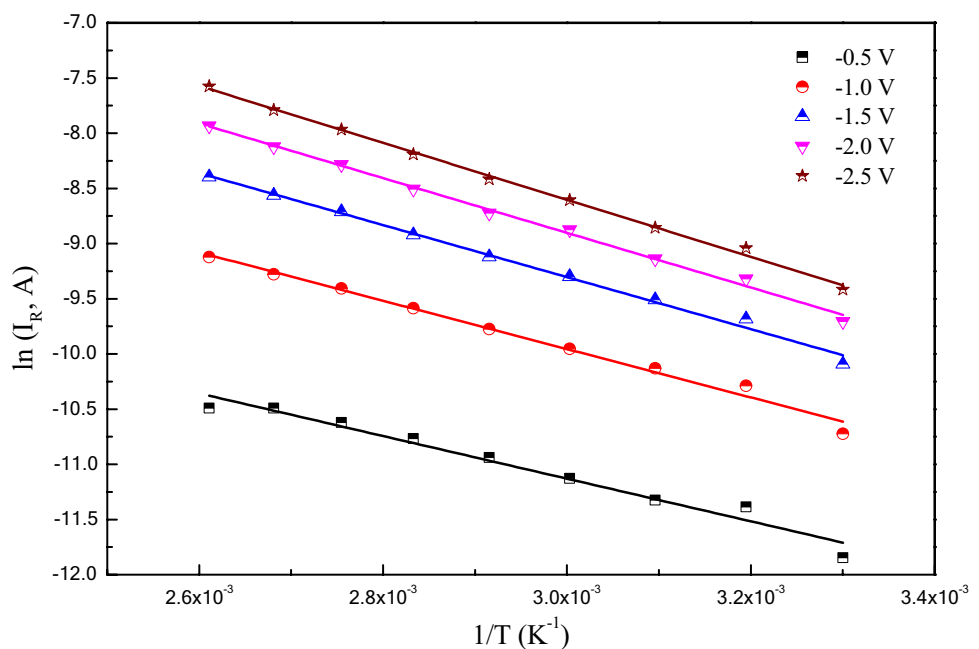
Fig.11 $\ln(I_R)$ versus $V_R^{1/2}$ for Al/NTCDA/p-Si/Al Schottky diode at different temperatures
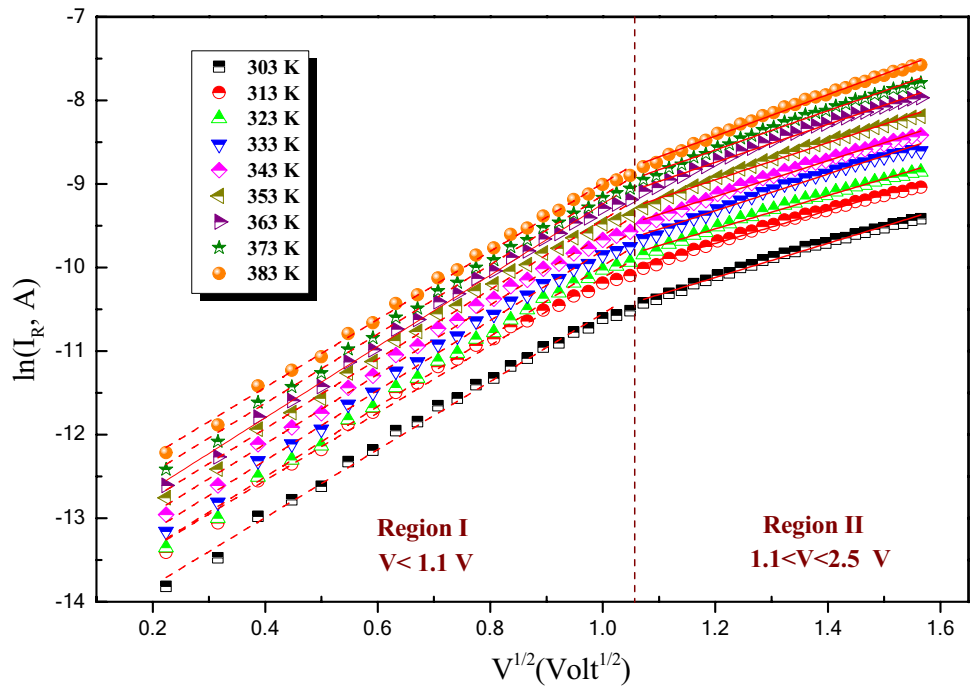
$$I_{Sc,R} = AA^*T^2 \exp\left(\frac{-\Phi_B}{k_B T}\right)\exp\left(\frac{\beta_{Sc} E^{1/2}}{k_B T}\right), \qquad (15)$$

where E is the applied electric field and β_{Sc} is the Schottky field lowering coefficient. On the basis of the Poole–Frenkel emission mechanism, the reverse current can be represented as follows [45, 77]:

$$I_{PF,R} = I_S A \exp\left(\frac{\beta_{PF} E^{1/2}}{k_B T}\right), \qquad (16)$$

where β_{PF} is the Poole–Frenkel coefficient. The value of β is given by [44, 77]:

$$\beta = \left(\frac{q^3}{b\pi\varepsilon\varepsilon_o}\right)^{1/2}, \qquad (17)$$

where b is a constant equals 1 for Poole–Frenkel mechanism and equals 4 for Schottky mechanism [45, 77], ε is the dielectric constant of the material ($\varepsilon = 2.89$ [72]), ε_o is permittivity of free space (8.85×10^{-12} F m^{-2}), and q is electron's charge. The calculated values of β were about 4.55×10^{-5} eV m$^{1/2}$ V$^{1/2}$ for the Poole–Frenkel mechanism and 2.28×10^{-5} eV m$^{1/2}$ V$^{1/2}$ for Schottky mechanism. The experimental values of β estimated from the slope of the straight lines in the region (**I**) and region (**II**) at room temperature were about 4.12×10^{-5} eV m$^{1/2}$ V$^{1/2}$ and 2.07×10^{-5} eV m$^{1/2}$ V$^{1/2}$, respectively. The difference between the calculated and experimental values of β may be due to either phonon-assisted tunneling through the barrier [75] or the small thickness

of the depletion region of Schottky in NTCDA film [69]. Hence, the transport mechanism in the low-voltage region (**I**) is interpreted as a Poole–Frenkel mechanism, while in the high-voltage region (**II**) is interpreted as a Schottky emission mechanism. Both Schottky and Poole–Frenkel's lowering coefficient are temperature-dependent parameters as observed from Fig. 12. This confirms that the phonon-assisted tunneling process is the main reason for the disagreement between the theoretical value and experimental values of β.

Furthermore, the series resistance of Schottky diode that arises from the contacts resistance and undepleted semiconductor resistance was calculated using modified Norde's function as follows [54, 78–80]:

$$F(V) = \frac{V}{\gamma} - \frac{k_B T}{q}\ln\left(\frac{I(V)}{AA^*T^2}\right), \qquad (18)$$

where γ is the first integer (dimensionless) number greater than the ideality factor estimated from thermionic emission calculations [54, 79, 80]. From the minimum value of Norde's function $F(V_o, I_o)$, the barrier height and series resistance were calculated using the following relations:

$$R_s = \frac{(\gamma - n)k_B T}{q I_o}, \qquad (19)$$

where I_o is the current value corresponds to the minimum value of Norde's function.

Fig.12 The temperature dependence of both Schottky and Poole–Frenkel lowering coefficients
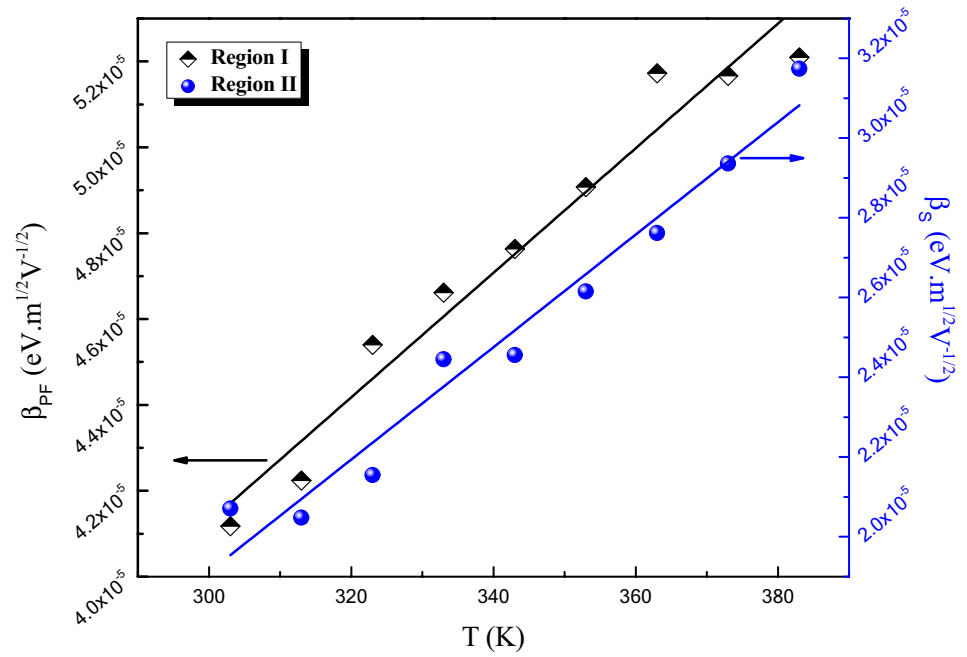

$$\Phi_B = qF(V_o, I_o) + \frac{qV_o}{\gamma} - k_B T. \tag{20}$$

Figure 13 shows the relation between the forward biasing voltage and Norde's function at different temperatures. The estimated values of series resistance and barrier height using Eqs. (19) and (20) are shown in Table 1. A clear decrement in the series resistance values with increasing the temperature is observed.

The presence of structural and/or surface defects and organic interfacial layer between the inorganic semiconductor substrate and metal electrode produces a high density of interface states. These states play a crucial role not only in Fermi-level pinning at metal/semiconductor contact but also in the alternation of SBH values and resulting in flow of

Fig.13 The voltage dependence of Norde's function of the fabricated Schottky diode at different temperatures
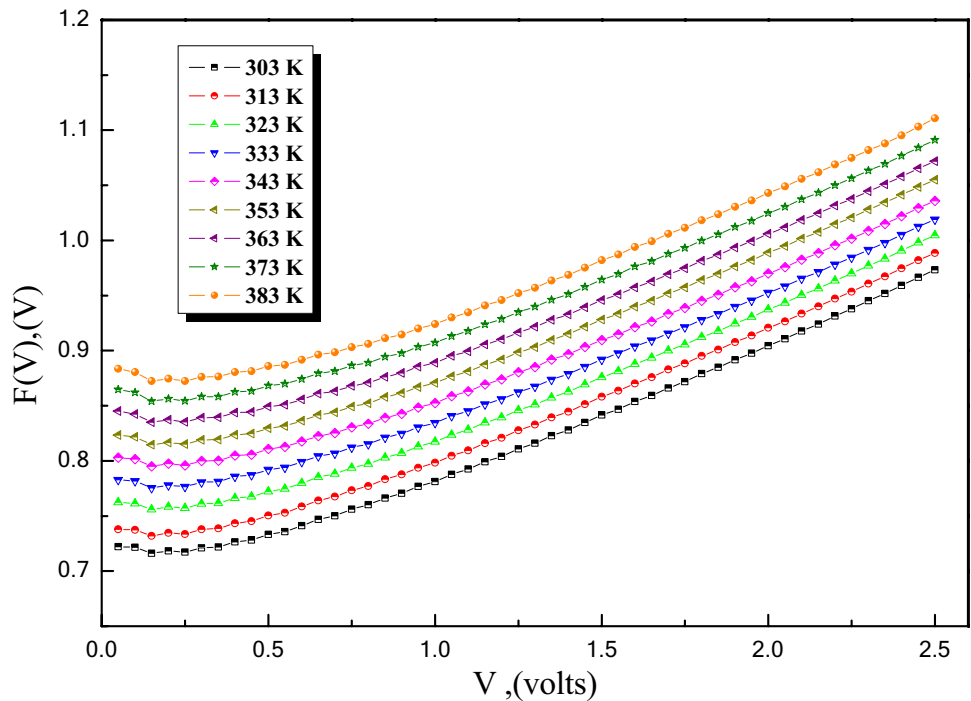
leakage current. Furthermore, the interaction between metal electrode evanescent wave function and those of organic thin-film would induce a new contribution of interface states known as the induced density of interface states, IDIS. According to Herbert Kroemer's statement in his Nobel lecture "often, it may be said that the interface is the device", and according to the essential function that engineering of interface states obtain in order to control the electrical performance of the Schottky barrier diode [61, 81–84], it was mandatorily task to give an overview of the pivotal role of NTCDA thin film on the passivation of the surface interface states and investigating their density distribution with respect to their energy. For this reason, the density of interface states, N_{ss}, as a function of its energy, E_{ss}, is calculated.

The voltage dependence of effective barrier height, Φ_e, is interrelated to the ideality factor as a function of voltage by the following relation [61, 81–84]:

$$\frac{d\Phi_e}{dV} = 1 - \frac{1}{n(V)}, \tag{21}$$

In case of insertion of a sufficiently thick organic layer, the ideality factor and interface states are related through the following relation [61, 81–84]:

$$\frac{1}{n(V)} = \frac{\varepsilon_i}{\varepsilon_i + q^2 N_{ss}\delta}, \tag{22}$$

where ε is the dielectric constant of the NTCDA layer and δ is its thickness. The effective barrier height is related to the estimated barrier height Φ_B by the following equation [61, 81–84]:

$$\phi_e = \phi_B + \left(1 - \frac{1}{n(V)}\right)V. \tag{23}$$

The interface states energy, E_{ss}, with respect to the topmost of p-type semiconductor valance band is expressed as follows [61, 81–84]:

$$E_{ss} - E_v = q(\phi_e - V). \tag{24}$$

Figure 14 reveals the exponential growth of the density of interface states in energy ranges from the middle of the gap to the top of the valance band for the fabricated device at different temperatures. It is noted that the density of states ranges from 4.3×10^{13} to 1.5×10^{14} eV^{-1} cm^{-2} and from 3.5×10^{13} to 1.3×10^{14} eV^{-1} cm^{-2} for 303 K and 383 K, respectively. The resulted values of N_{ss} are comparable to the obtained values in the previous work [83, 84] and higher than that was obtained by ref [85].

It can be noticed from Fig. 14 that the distribution of interface states density that exists in charge-neutral level, CNL, above Fermi level as shown in Fig. 15 at a certain temperature decreases as their energy position shifts away from the top of valance band till it reaches an optimum value where the density of interface states reach a minimum value and then begin to increase again. Moreover, the temperature shows a significant impact on the passivation of interface states, whereas the temperature increases, the density of interface states decreases slightly and the optimum value energy position shifts upward away from the top of the valance band. The obtained temperature dependence of the interface state density was previously observed at Er/p-InP

Fig.14 The distribution of interface states for Al/NTCDA/p-Si/Al Schottky diode at different temperatures and the inset shows the purposed interaction of NTCDA with Si surface dangling bonds
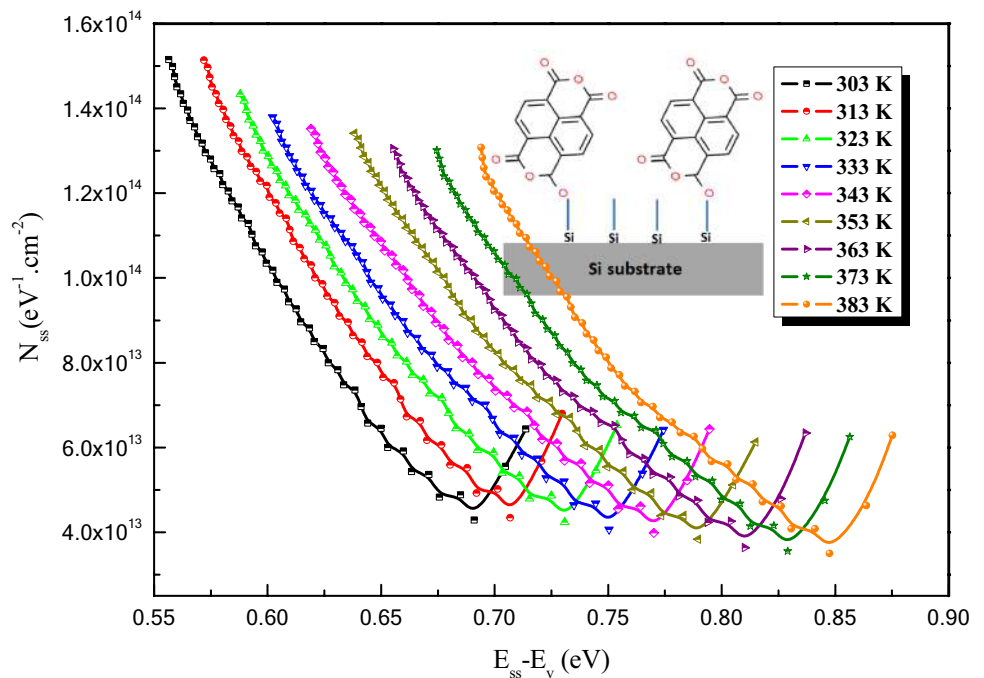
Fig.15 The purposed energy-band diagram of the fabricated Schottky diode under thermal equilibrium condition
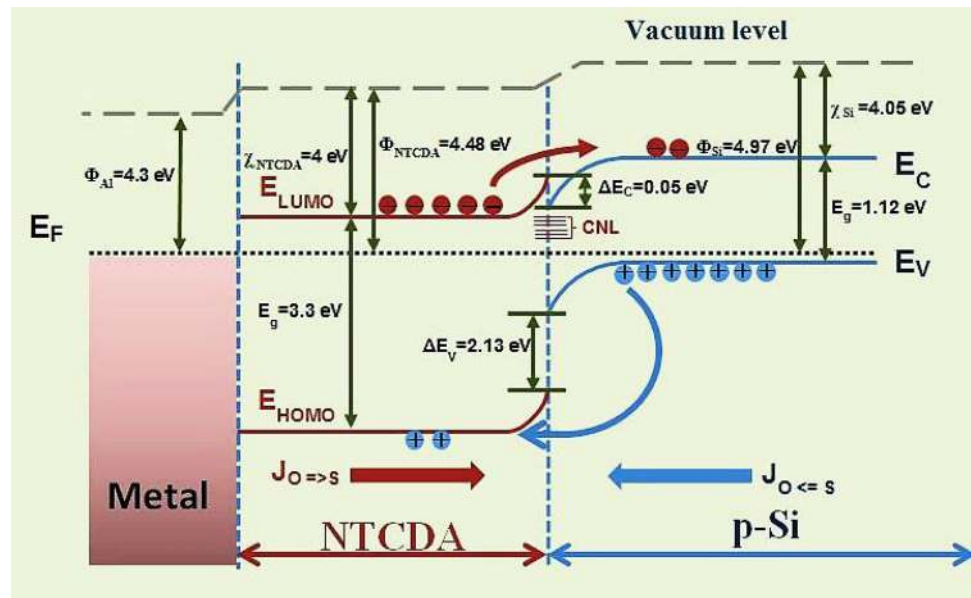
Schottky diode [86] and V(200 Å)/Pd(300 Å)/InP Schottky diode [87]. This passivation process is useful for decreasing the effect of interface states on trapping the excited charge carriers, reducing the minority charge carriers' lifetime and deteriorating the tunneling routes that were added by these states. Moreover, the passivation process would control the role of interface states in quenching the electron–hole pairs and hence increasing the photocurrent of any optoelectronic device. The passivation of interface states density of AL/NTCDA/p-Si under the influence of temperature is convenient to the results of the series resistance decrease of the fabricated Schottky diode with increasing temperature.

The offset between the conduction band of p-Si and LUMO energy limits the migration of electron from the conduction band of p-Si to LUMO of NTCDA, hence decreasing the recombination at the electrode. The passivation process involves the passivation of the dangling bonds on the Si substrate's surface. It may be proposed that after depositing NTCDA thin film, the dangling bonds of Si surface would be interacted with oxygen atom of the acyl groups in NTCDA due to the high chemical affinity of Si to oxygen through a covalent bond resulting in partial passivation as depicted in the inset of Fig. 14. This passivation would decrease the density of interface states which act as electron–hole recombination sites [88]. Hence, NTCDA acted as a partial passivation layer in addition to conserving the conjugation characteristics.

Consider the case, where organic and inorganic semiconductors that are different in work function, energy gap, and electron affinity are brought together forming an organic/inorganic heterojunction, the valance band of inorganic and HOMO of organic will offset by a discontinuity, ΔE_V, while the conduction band of inorganic and LUMO of organic will offset by, ΔE_C [53]. These discontinuities depend on the difference in the energy gap of both, $\Delta E_g = E_g(Si) - E_g(NTCDA)$, and energy that the electron should have to leave the conduction or LUMO of inorganic or organic, respectively, to vacuum level, the electron affinity, χ. Figure 15. reveals the purposed energy diagram of the fabricated Schottky diode. The non-applicability of the concept of charge flow from the low to the high work function side in organic/inorganic interfaces means leads to the alignment of the vacuum level ($\Delta = 0$) according to Schottky–Mott rule or Anderson rule [53, 89].

According to Anderson rule [53, 89] and based on the known values of silicon energy gap ($E_{g\,Si} = 1.12$ eV), electron affinity ($\chi_{Si} = 4.05$ eV), and work function ($\Phi_{Si} = 4.97$ eV) [90] and with the help of the previously estimated values of NTCDA frontiers molecular orbitals parameters such as electron affinity ($\chi_{NTCDA} = 4$ eV) [91] and energy gap ($E_{g\,NTCDA} = 3.3$ eV) [92], the discontinuities ΔE_V and ΔE_C are estimated, where ($\Delta E_C = \chi_{Si} - \chi_{NTCDA}$) and ($\Delta E_V = \Delta E_g - \Delta E_C$)[53] and expressed on Fig. 15. Moreover, the work function of NTCDA is estimated from the built-in potential, V_{bi}, barrier height, Φ_B, and, V_p, which represents the difference in potential between Fermi level and the valance band top by the following equation [53]:

$$V_{bi} = \Phi_{Si} - \Phi_{NTCDA} = \Phi_B - V_P, \qquad (25)$$

Taking into account that the value of V_p was estimated to be 0.228 eV [53] and Φ_B equals 0.72 eV, the work function of NTCDA is calculated and found to 4.48 eV. Since the work function and electron affinity of silicon are greater than these of NTCDA, while NTCDA has a wider energy gap than that of silicon, and hence, the fabricated

device behaves as an accumulating heterojunction. Under thermal equilibrium and zero-biasing, the major charge carriers of NTCDA will be transported by Thermionic emission through the barrier between the heterojunction, while the minor charge carriers would tunnel through the barrier. Since the valance band offset is larger than conduction band offset, hence the current flow through the fabricated device will be predominantly determined by the electron flow from NTCDA to p-Si [93]. The obtained behavior of I–V curve depicted in Fig. 3 is a result of charge carriers' diffusion in CNL region beside the charges recombination at the space charge region at the interface. The interface states that exist in the CNL region will play a significant role in the recombination probability between the generated electron–hole pairs [89].

4 Conclusion

The performance of MIS Schottky diode was investigated with the existence of 1,4,5,8 naphthalenetetracarboxylic dianhydride, NTCDA, thermally evaporated thin film as an interlayer between the top Al electrode and the p-Si substrate. The structural and topographical properties of the fabricated film were investigated and showed the nanostructured nature of the film and the low values of surface roughness. Furthermore, both barrier height, ideality factor, and the series resistance of the present architecture were calculated at different temperatures. The charge carriers' conduction mechanism within the fabricated device is found to be SCLC conduction in forward biasing. The density of interface states is estimated and found to be in the range $(4.3 \times 10^{13}$–$1.5 \times 10^{14})$ eV^{-1} cm^{-2} and $(3.5 \times 10^{13}$–$1.3 \times 10^{14})$ eV^{-1} cm^{-2} for 303 K and 383 K, respectively. The energy shift of N_{ss} distribution under the influence of temperature was interpreted in terms of surface passivation of Si surface defects. This confirms that the peripheral temperature tunes the performance of the present architecture which suggests this device as a temperature sensor. The sensitivity of the fabricated device as a temperature sensor was evaluated in terms of the temperature coefficient of current and found to range from 1.24 to 0.92% K^{-1} at voltage range from 0.5 to 2.5 V, while the temperature coefficient of voltage was ranged from -0.59 to -0.41% K^{-1} at current range from 0.1 to 0.5 mA.

References

1. M.V. Jacob, Organic semiconductors: past, present and future. Electronics **3**, 594–597 (2014)
2. J.D. Myers, J. Xue, Organic semiconductors and their applications in photovoltaic devices. Polym Rev **52**, 1–37 (2012)
3. V. Coropceanu, H. Li, P. Winget, L. Zhu, J.-L. Bredas, Electronic-structure theory of organic semiconductors: charge-transport parameters and metal/organic interfaces. Ann. Rev. Mater. Res. **43**(1), 63–87 (2013)
4. A. Ahmadiv, B. Gerislioglu, Z. Ramezani, Generation of magnetoelectric photocurrents using toroidal resonances: a new class of infrared plasmonic photodetectors. Nanoscale **11**, 13108–13116 (2019)
5. P. Martyniuk, J. Antoszewski, M. Martyniuk, L. Faraone, A. Rogalski, New concepts in infrared photodetector designs. Appl. Phys. Rev. **1**, 041102 (2014)
6. V. Coropceanu, J. Cornil, D.A. da Silva Filho, Y. Olivier, R. Silbey, J.-L. Brédas, Charge transport in organic semiconductors. Chem. Rev. **107**, 926–952 (2007)
7. C. Groves, Simulating charge transport in organic semiconductors and devices: a review. Rep. Prog. Phys. **80**, 026502–026538 (2017)
8. M. Häming, A. Schöll, E. Umbach, F. Reinert, Adsorbate-substrate charge transfer and electron-hole correlation at adsorbate/metal interfaces. Phys. Rev. B **85**, 235132–235144 (2012)
9. J. Ziroff, S. Hame, M. Kochler, A. Bendounan, A. Schöll, F. Reinert, Low-energy scale excitations in the spectral function of organic monolayer systems. Phys. Rev. B **85**, 161404–161408 (2012)
10. A. Bendounan, F. Forster, A. Schöll, D. Batchelor, J. Ziroff, E. Umbach, F. Reinert, Electronic structure of 1 ML NTCDA/Ag(111) studied by photoemission spectroscopy. Surf. Sci. **601**, 4013–4017 (2007)
11. S.M. Barlow, R. Raval, Complex organic molecules at metal surfaces: bonding, organisationand chirality. Surf. Sci. Rep. **50**, 201–341 (2003)
12. C. Stadler, S. Hansen, A. Schöll, T.-L. Lee, J. Zegenhagen, C. Kumpf, E. Umbach, Molecular distortion of NTCDA upon adsorption on Ag(111): a normal incidence x-ray standing wave study. New J. Phys. **9**, 50–58 (2007)
13. R. Tonner, P. Rosenow, P. Jakob, Molecular structure and vibrations of NTCDA monolayers on Ag(111) from density-functional theory and infrared absorption spectroscopy. Phys. Chem. Chem. Phys. **18**, 6316–6328 (2016)
14. S. Kera, S. Tanaka, H. Yamane, D. Yoshimura, K.K. Okudaira, K. Seki, N. Ueno, Quantitative analysis of photoelectron angular distribution of single-domain organic monolayer film: NTCDA on GeS(001). Chem. Phys. **325**, 113–120 (2006)
15. A.S. Komolov, P.J. Møller, Y.G. Aliaev, E.F. Lazneva, S. Akhremtchik, F.S. Kamounah, J. Mortensen, K. Schaumburg, Organic–organic interfaces and unoccupied electronic states of thin films of perylene and naphthalene derivatives. J. Mol. Struct. **744–747**, 145–149 (2005)
16. H. Tachikawa, H. Kawabata, A density functional theory study on the degradation mechanism of thin film of organic semiconductor by water molecules. Thin Solid Films **516**, 3287–3293 (2008)
17. H. Tachikawa, H. Kawabata, Electronic states of alkali metal-NTCDA complexes: a DFT study. Solid State Sci. **48**, 141–146 (2015)
18. X. Han, F. Yi, T. Sun, J. Sun, Synthesis and electrochemical performance of Li and Ni 1,4,5,8-naphthalenetetracarboxylates as anodes for Li-ion batteries. Electrochem. Commun. **25**, 136–139 (2012)

19. E.R. Triboni, M.F.P. Da Silva, A.T. Finco, M.A. Rodrigues, G.J.-F. Demets, F.H. Dyszy, P.C. Isolani, P.B. Filho, M.J. Politi, Synthesis and properties of new paramagnetic hybrid bayerite from Al(0)/naphthalene dianhydride reaction. Mater. Res. **13**(4), 505–511 (2010)

20. S. Tanida, K. Noda, H. Kawabata, K. Matsushige, N-channel thin-film transistors based on 1,4,5,8-naphthalene tetracarboxylic dianhydride with ultrathin polymer gate buffer layer. Thin Solid Films **518**, 571–574 (2009)

21. W.T. Hammond, J.P. Mudrick, J. Xue, Balancing high gain and bandwidth in multilayer organic photodetectors with tailored carrier blocking layers. J. Appl. Phys. **116**, 214501–214508 (2014)

22. M. Hiramoto, A. Miki, M. Yoshida, M. Yokoyama, Photocurrent multiplication in organic single crystals. Appl. Phys. Lett. **81**(8), 1500–1502 (2002)

23. L. Torsi, A. Dodabalapur, N. Cioffi, L. Sabbatini, P.G. Zambonin, NTCDA organic thin-film-transistor as humidity sensor: weaknesses and strengths. Sens. Actuators B. **77**, 7–11 (2001)

24. H.E. Katz, A.J. Lovinger, J. Johnson, C. Kloc, T. Siegrist, W. Li, Y.-Y. Lin, A.A. Dodabalapur, Soluble and air-stable organic semiconductor with high electron mobility. Nature **404**(30), 478–480 (2000)

25. S.T. Pérez-Merchancano, G.E. Marques, L.E. Bolivar-Marinez, Optical transitions in new trends organic materials. Microelectron. J. **39**, 576–578 (2008)

26. H. Abdel-Khalek, E. Shalaan, M. Abd- El Salam, A.M. El-Sagheer, A.M. El-Mahalawy, Effect of thermal annealing on structural, linear and nonlinear optical properties of 1,4,5,8-naphthalene tetracarboxylic dianhydride thin films. J. Mol. Struct. **1178**, 408–419 (2019)

27. T. Gerbich, H.-C. Schmitt, I. Fischer, J. Petersen, J. Albert, R. Mitrić, A time-resolved study of 1,8-naphthalic anhydride and 1,4,5,8-naphthalene-tetracarboxylic dianhydride. J. Phys. Chem. A. **119**(23), 6006–6016 (2015)

28. C. Falkenberg, C. Uhrich, B. Maennig, M.K. Riede, K. Leo, 1,4,5,8-Naphthalenetetracarboxylic dianhydride as transparent electron transport material in organic p-i-n solar cells. Proc. SPIE. **6999**, 69990S-1–69990S-8 (2008).

29. B.E. Lassiter, G. Wei, S. Wang, J.D. Zimmerman, V.V. Diev, M.E. Thompson, S.R. Forrest, Organic photovoltaics incorporating electron conducting exciton blocking layers. Appl. Phys. Lett. **98**, 243307–243309 (2011)

30. M. Zhu, G. Liang, T. Cui, K. Varahramyan, Depletion-mode n-channel organic field-effect transistors based on NTCDA. Solid-State Electron. **47**, 1855–1858 (2003)

31. L. Torsi, Novel applications of organic based thin film transistors. Microelectron. Reliab. **40**, 779–782 (2000)

32. L. Torsi, A. Dodabalapur, L. Sabbatini, P.G. Zambonin, Multiparameter gas sensors based on organic thin-film-transistors. Sens. Actuators B. **67**, 312–316 (2000)

33. G. Liang, T. Cui, K. Varahramyan, Electrical characteristics of diodes fabricated with organic semiconductors. Microelectron. Eng. **65**, 279–284 (2003)

34. T. Katsume, M. Hiramoto, M. Yokoyama, Photocurrent multiplication in naphthalene tetracarboxylic anhydride film at room temperature. Appl. Phys. Lett. **69**, 3722–3724 (1996)

35. S.R. Forrest, F.F. So, Organic optoelectronic devices and methods. US patent 5315129 May 24 (1994)

36. K.-S. Kim, S.-C. Park, J.-G. Nam, M. Hiramoto, Organic photoelectric conversion film, and photoelectric conversion device and image sensor each having the organic photoelectric conversion film. US patent 2009/0294761 A1 (2009)

37. Y.-M. Koo, O.-K. Song, Spontaneous charge transfer from indium tin oxide to organic molecules for effective hole injection. Appl. Phys. Lett. **94**, 153302–153304 (2009)

38. Z. Jehl, M. Bouttemy, D. Lincot, J.F. Guillemoles, I. Gerard, A. Etcheberry, G. Voorwinden, M. Powalla, N. Naghavi, Insights on the influence of surface roughness on photovoltaic properties of state of the art copper indium gallium diselenide thin films solar cells. J. Appl. Phys. **111**, 114509–114515 (2012)

39. M. Zawodzki, R. Resel, M. Sferrazza, O. Kettner, B. Friedel, Interfacial morphology and effects on device performance of organic bilayer heterojunction solar cells. ACS Appl. Mater. Interfaces **7**(30), 16161–16168 (2015)

40. S.-Y. Lien, Y.-S. Cho, Y. Shao, C.-H. Hsu, C.-C. Tsou, W. Yan, P. Han, D.-S. Wuu, Influence of surface morphology on the effective lifetime and performance of silicon heterojunction solar cell. Int. J. Photoenergy **2015**, 1–8 (2015)

41. D. Benmoussa, B. Meriem, K. Hamid, O.-A. Amaria, Study the effect of surface recombination velocity on performance of solar cells based sige. 4th international conference on automation, control engineering and computer science (ACCS-2017). Proc. Eng. Technol. **19**, 78–81 (2017)

42. P. Zhang, Effects of surface roughness on electrical contact, RF heating and field enhancement. Ph.D. Dissertation, The University of Michigan, USA (2012)

43. O.S. Cifci, M. Bakir, J.L. Meyer, A. Kocyigit, Morphological and electrical properties of ATSP/p-Si photodiode. Mat. Sci. Semicond. Proc. **74**, 175–182 (2018)

44. J. Zhou, J. Huang, Photodetectors based on organic–inorganic hybrid lead halide perovskites. Adv. Sci. **5**, 1700256–1700279 (2018)

45. M.M. Makhlouf, M.M. El-Nahass, M.H. Zeyada, Fabrication, temperature dependent current-voltage characteristics and photoresponse properties of Au/α-PbO2/p-Si/Al heterojunction photodiode. Mat. Sci. Semicond. Proc. **58**, 68–75 (2017)

46. K.V. Chizh, V.A. Chapnin, V.P. Kalinushkin, V.Y. Resnik, M.S. Storozhevykh, V.A. Yuryev, Metal silicide/poly-Si Schottky diodes for uncooled microbolometers. Nanosc. Res. Lett. **8**, 177 (2013)

47. A.G. Imer, Y.S. Ocak, Effect of light intensity and temperature on the current voltage characteristics of Al/SY/p-Si organic–inorganic heterojunction. J. Electron. Mater. **45**(10), 5347–5355 (2016)

48. J. Lee, T. Uhrmann, T. Dimopoulos, H. Bruckl, J. Fidler, TEM study on diffusion process of NiFe Schottky and MgO/NiFe tunneling diodes for spin injection in silicon. IEEE Trans. Magn. **46**, 2067–2069 (2010)

49. A. Tataroğlu, F.Z. Pür, The Richardson constant and barrier inhomogeneity at Au/Si$_3$N$_4$/n-Si (MIS) Schottky diodes. PhysicaScripta **88**, 15801–15806 (2013)

50. Z. Yuan, A photodiode with high rectification ratio and low turn-on voltage based on ZnO nanoparticles and SubPc planar heterojunction. Phys. E **56**, 160–164 (2014)

51. N.P. Maity, R. Maity, R.K. Thapa, S. Baishya, Image force effect on tunneling current for ultrathin high-K dielectric material Al$_2$O$_3$ based metal oxide semiconductor devices. J. Nanoelectron. Optoelectron. **10**, 645–648 (2015)

52. M.A. Mayimele, J.P.J. Van Rensburg, F.D. Auret, M. Diale, Analysis of temperature dependant current-voltage characteristics and extraction of series resistance in Pd/ ZnO Schottky barrier diodes. Phys. B Condens. Matter. **480**, 58–62 (2016)

53. H.M. Zeyada, M.M. El-Nahass, M.M. El-Shabaan, Photovoltaic properties of the 4H-pyrano[3,2-c]quinoline derivatives and their applications in organic–inorganic photodiode fabrication. Synth. Methods **220**, 102–113 (2016)

54. H. Abdel-Khalek, E. Shalaan, M. Abd-El Salam, A. M. El-Mahalawy, Effect of illumination intensity on the characteristics of Cu(acac)2/n-Si photodiode. Synth. Methods 245, 223–236 (2018).

55. S. Mahato, D. Biswas, L.G. Gerling, C. Voz, J. Puigdollers, Analysis of temperature dependent current–voltage and capacitance–voltage characteristics of an Au/V_2O_5/n-Si Schottky diode. AIP Adv. **7**, 085313 (2017)

56. D. Zhu, J. Xu, A.N. Noemaun, J.K. Kim, E.F. Schubert, M.H. Crawford, D.D. Koleske, The origin of the high diode-ideality factors in GaInN/GaN multiple quantum well light-emitting diodes. Appl. Phys. Lett **94**, 081113 (2009)

57. S. Mahato, Composition analysis of two different PEDOT:PSS commercial products used as an interface layer in Au/n-Si Schottky diode. RSC Adv. **7**, 47125–47131 (2017)

58. R.K. Gupta, K. Ghosh, P.K. Kahol, Fabrication and electrical characterization of Au/p-Si/STO/Au contact. Curr. Appl. Phys. **9**, 933–936 (2009)

59. J. Osvald, Temperature dependence of barrier height parameters of inhomogeneous Schottky diodes. Microelectron. Eng. **86**, 117–120 (2009)

60. A. Tombak, Y.S. Ocak, S. Asubay, T. Kilicoglu, F. Ozkahraman, Fabrication and electrical properties of an organic-inorganic device based on Coumarin 30 dye. Mat. Sci. Semicond. Proc. **24**, 187–192 (2014)

61. I. Hussain, M.Y. Soomro, N. Bano, O. Nur, M. Willander, Systematic study of interface trap and barrier inhomogeneities using I-V-T characteristics of Au/ZnOnanorods Schottky diode. J. Appl. Phys. **113**, 234509–234515 (2013)

62. T. Tunç, Ş. Altindal, İ. Uslu, İ. Dökme, H. Uslu, Temperature dependence current-voltage (I–V) characteristics of Au/n-S (111) Schottky barrier diodes with PVA (Ni, Zn-doped) interfacial layer. Mat. Sci. Semicond. Proc. **14**, 139–145 (2011)

63. R.D. Gould, The interpretation of space-charge-limited currents in semiconductors and insulators. J. Appl. Phys. **53**(4), 3353–3355 (1982)

64. N.F. Mott, R.W. Gurney, *Electronic Processes in Ionic Crystals* (Oxford University Press, London, 1940)

65. H.S. Soliman, A.A.M. Farag, N.M. Khosifan, T.S. Solami, Electronic and photovoltaic properties of Au/pyronine G(Y)/p-GaAs/Au: Zn heterojunction. J. Alloys Compd. **530**, 157–163 (2012)

66. M.M. El-Nahass, H.S. Metwally, H.E.A. El-Sayed, A.M. Hassanien, Electrical and photovoltaic properties of FeTPPCl/p-Si heterojunction. Synth. Methods **161**, 2253–2258 (2011)

67. H.M. Zeyada, M.M. El-Nahass, E.M. El-Menyawy, A.S. El-Sawah, Electrical and photovoltaic characteristics of indium phthalocyanine chloride/p-Si solar cell. Synth. Methods **207**, 46–53 (2015)

68. H.A. Afify, M.M. El-Nahass, A.-S. Gadallah, M.A. Khedr, Carrier transport mechanisms and photodetector characteristics of Ag/TiOPc/p-Si/Al hybrid heterojunction. Mat. Sci. Semicond. Proc. **39**, 324–331 (2015)

69. M.A. Lampert, Volume-controlled current injection in insulators. Rep. Prog. Phys. **27**, 329–367 (1964)

70. M.A. Lampert, Simplified theory of space-charge-limited currents in an insulator with traps. Phys. Rev. **103**, 1648–1656 (1956)

71. I.S. Yahia, G.B. Sakr, T. Wojtowicz, G. Karczewski, p-ZnTe/n-CdMnTe/n-GaAs diluted magnetic diode for photovoltaic applications. Semicond. Sci. Technol. **25**, 095001–095008 (2010). https://doi.org/10.1088/0268-1242/25/9/095001

72. P.K. Nayak, N. Periasamy, Calculation of electron affinity, ionization potential, transport gap, optical band gap and exciton binding energy of organic solids using 'solvation' model and DFT. Org. Electron. **10**, 1396–1400 (2009)

73. C.H. Kim, O. Yaghmazadeh, Y. Bonnassieux, G. Horowitz, Modeling the low-voltage regime of organic diodes: origin of the ideality factor. J. Appl. Phys. **110**, 093722 (2011)

74. S.R. Forrest, Organic–inorganic semiconductor devices and 3,4,9,10 perylenetetracarboxylicdianhydride: an early history of organic electronics. J. Phys. Condens. Matter **15**, S2599–S2610 (2003)

75. P. Pipinys, V. Lapeika, Analysis of reverse-bias leakage current mechanisms in metal/GaN Schottky diodes. Adv. Condens. Matter Phys. (2010). https://doi.org/10.1155/2010/526929

76. H.M. Zeyada, M.I. Youssif, N.A. El-Ghamaz, M.A. Nasher, Carrier transport mechanisms and photovoltaic characteristics of Au/toluidine blue/n-Si/Al heterojunction solar cell. J. Mater. Sci. Mater. Electron. **29**, 3592–3601 (2018)

77. A.M. Nawar, M.M. Makhlouf, Au-nanoparticles doped SiO_2 interfacial layer to promote the photovoltaic characteristics of Au/p-Si/Al solar cells. J. Alloys Compd. **767**, 1271–1281 (2018)

78. V. Aubry, F. Meyer, Schottky diodes with high series resistance: limitations of forward I–V methods. J. Appl. Phys. **76**, 7973–7984 (1994)

79. H. Norde, A modified forward I–V plot for Schottky diodes with high series resistance. J. Appl. Phys. **50**, 5052–5053 (1979)

80. K. Sato, Y. Yasumura, Study of forward I–V plot for Schottky diodes with high series resistance. J. Appl. Phys. **58**, 3655–3657 (1985)

81. A.M. Cowley, S.M. Sze, Surface states and barrier height of metal-semiconductor systems. J. Appl. Phys. **36**, 3212 (1965)

82. B. Boyarbay, H. Çetin, A. Uygun, E. Ayyildiz, Electrical characterization and fabrication of organic/inorganic semiconductor heterojunctions. Appl. Phys. A **103**, 89–96 (2011)

83. A. Ugur, A.G. Imer, Y.S. Ocak, Electrical and photoelectrical characterization of an organic–inorganic heterojunction based on quinolone yellow dye. Mat. Sci. Semicond. Proc. **39**, 569–574 (2015)

84. E. Elgazzar, A. Tataroğlu, A.A. Al-Ghamdi, Y. Al-Turki, W.A. Farooq, F. El-Tantawy, F. Yakuphanoglu, Thermal sensors based on delafossite film/p-silicon diode for low-temperature measurements. Appl. Phys. A **122**, 617–625 (2016)

85. K. Akkılıç, Y.S. Ocak, T. Kılıçoğlu, S. İlhan, H. Temel, Calculation of current-voltage characteristics of a Cu (II) complex/n-Si/AuSb Schottky diode. Curr. Appl. Phys. **10**, 337–341 (2010)

86. L. Dasaradha Rao, N. Ramesha Reddy, A. Ashok Kumar, V. Rajagopal Reddy, Temperature dependent electrical properties of rare-earth metal Er Schottky contact on p-type InP. AIP Conf. Proc. **1536**, 471–472 (2013)

87. S. Sankar Naik, V. Rajagopal Reddy, Temperature dependency and current transport mechanisms of Pd/V/n-type InPschottky rectifiers. Adv. Mat. Lett. **3**(3), 188–196 (2012)

88. S. Avasthi, Y. Qi, G.K. Vertelov, J. Schwartz, A. Kahn, J.C. Sturm, Silicon surface passivation by an organic overlayer of 9,10-phenanthrenequinone. Appl. Phys. Lett. **96**, 222109 (2010)

89. A. Vilan, D. Cahen, Chemical modification of semiconductor surfaces for molecular electronics. Chem. Rev. **117**, 4624–4666 (2017)

90. S.M. Sze, *Physics of Semiconductors Devices* (Wiely, New York, 1969)

91. P.K. Nayak, N. Periasamy, Calculation of electron affinity, ionization potential, transport gap, optical band gap and exciton binding energy of organic solids using solvation model and DFT. Org Electron **10**, 1396–1400 (2009)

92. A. Nollau, M. Pfeiffer, T. Fritz, K. Leo, Controlled n-type doping of a molecular organic semiconductor: naphthalenetetracarboxtlic dianhydride (NTCDA) doped with bis (ethylenedithio)-tetrathiafulvalene (BEDT-TTF). J. Appl. Phys. **87**, 4340 (2000)

93. D. Somvanshi, S. Jit, Analysis of temperature-dependent electrical characteristics of n-ZnO nanowires (NWs)/p-Si heterojunction diodes. IEEE Trans. Nanotechnol. **13**(1), 62–69 (2014)